

Interfaces and Materials in Lithium Ion Batteries: Challenges for Theoretical Electrochemistry

Johannes Kasnatscheew¹ · Ralf Wagner² · Martin Winter^{1,2} · Isidora Cekic-Laskovic^{1,2}

Received: 21 June 2017 / Accepted: 9 April 2018 / Published online: 18 April 2018
© Springer International Publishing AG, part of Springer Nature 2018

Abstract Energy storage is considered a key technology for successful realization of renewable energies and electrification of the powertrain. This review discusses the lithium ion battery as the leading electrochemical storage technology, focusing on its main components, namely electrode(s) as active and electrolyte as inactive materials. State-of-the-art (SOTA) cathode and anode materials are reviewed, emphasizing viable approaches towards advancement of the overall performance and reliability of lithium ion batteries; however, existing challenges are not neglected. Liquid aprotic electrolytes for lithium ion batteries comprise a lithium ion conducting salt, a mixture of solvents and various additives. Due to its complexity and its role in a given cell chemistry, electrolyte, besides the cathode materials, is identified as most susceptible, as well as the most promising, component for further improvement of lithium ion batteries. The working principle of the most important commercial electrolyte additives is also discussed. With regard to new applications and new cell chemistries, e.g., operation at high temperature and high voltage, further improvements of both active and inactive materials are inevitable. In this regard, theoretical support by means of modeling, calculation and simulation approaches can be very helpful to ex ante pre-select and identify the aforementioned components suitable

This article is part of the Topical Collection “Modeling Electrochemical Energy Storage at the Atomic Scale”; edited by “Martin Korth”.

✉ Johannes Kasnatscheew
j.kasnatscheew@fz-juelich.de

✉ Isidora Cekic-Laskovic
i.cekcic-laskovic@uni-muenster.de

¹ Helmholtz-Institute Münster, IEK-12, Forschungszentrum Jülich GmbH, Corrensstrasse 46, 48149 Münster, Germany

² MEET Battery Research Center/Institute of Physical Chemistry, University of Münster, Corrensstrasse 46, 48149 Münster, Germany

for a given cell chemistry as well as to understand degradation phenomena at the electrolyte/electrode interface. This overview highlights the advantages and limitations of SOTA lithium battery systems, aiming to encourage researchers to carry forward and strengthen the research towards advanced lithium ion batteries, tailored for specific applications.

Keywords Electrochemical energy storage · Lithium ion battery · Electrode materials · Electrolyte · Electrolyte/electrode interface · Computational chemistry

1 Terminology

The following definitions are used within the review.

Term	Description
Active materials	Active materials participate in the electrochemical charge/discharge reaction in a cell
Adsorption	“An increase of the concentration of a solute in the vicinity of a solid surface, over that in the bulk of the solution, due to the attractive interaction between the solid immersed into the solution and the solute. Adsorption on a solid from a gaseous phase also occurs. It is generally considered to be a physical process” [1]
Alloy	An alloy consists of mixed metallic or intermetallic phases with no ordered structure
Anode	“The electrode where oxidation occurs in an electrochemical cell. It is the positive electrode in an electrolytic cell, while it is the negative electrode in a galvanic cell” [1]
Battery	“A device that stores electrical energy using electrochemical cells. Strictly speaking, a battery should consist of several, internally connected, electrochemical cells. However, in present usage all storage devices (single cell and multiple cell) are called batteries” [1]
Cathode	“The electrode where reduction occurs in an electrochemical cell. It is the negative electrode in an electrolytic cell, while it is the positive electrode in a galvanic cell” [1]
Cell voltage	“The electrical potential difference between the two electrodes of an electrochemical cell” [1]
Concentration polarization	“The polarization associated with the diffusional transport of the reactants to the electrode surface from the bulk of the electrolyte and the reverse transport of the products” [1]
Electrochemical cell	“A device that converts chemical energy into electrical energy or vice versa when a chemical reaction is occurring in the cell” [1]; “It can be either a galvanic cell, when the reactions are spontaneous, or an electrolytic cell, when the reactions are non-spontaneous” [2]
Electrode	“The two electronically conducting parts of an electrochemical cell. These can be simple metallic structures or much more complicated, composite structures” [1]

Term	Description
Electrolytic cell	“An electrochemical cell that converts electrical energy into chemical energy. The chemical reactions do not occur “spontaneously” at the electrodes when they are connected through an external circuit. The reaction must be forced by applying an external electrical current. It is used to store electrical energy in chemical form (rechargeable battery). It is also used to decompose or produce new chemicals by application of electrical power (electrolysis)” [1]
Galvanic (voltaic) cell	“An electrochemical cell that converts chemical energy into electrical energy. A cell in which chemical reactions occur spontaneously at the electrodes when they are connected through an external circuit, producing an electrical current” [1]
Half cell	“A somewhat archaic term, indicating a structure that contains an electrode and the surrounding electrolyte” [1]
Inactive materials	Inactive materials do not contribute to the energy storage related redox chemistry of the cell
Interface and interphase	“The inhomogeneous spacial region at the interface between two bulk phases in contact. The “interface” is a two-dimensional surface, while the “interphase” is a thin, but three-dimensional, volume” [1]
Intermetallic phase	An intermetallic phase has a defined stoichiometry and structure in an at least binary system of metals
Joule heating	Process whereby the energy of an electric current is converted into heat as it flows through a resistance
Mass transport	“The phenomenon of movement (transportation) of mass (in the form of molecules or ions) from one part of the system to another. This occurs through convection, diffusion, or electro migration” [1]
Oxidation	“The process in which a chemical species loses one or more electrons; it is the reversed process to the reduction” [2]
Redox couple	“Chemical species that has at least two oxidation states, and thus can act either as the reduced or the oxidized species (depending on the oxidation state)” [2]
Redox reaction	“A class of electrode reactions involving oxidation/reduction of two dissolved species” [1]
Reduction	“A process in which a chemical species gains one or more electrons; reversed process is called oxidation” [2]
Standard hydrogen electrode (SHE)	The IUPAC (International Union of Pure and Applied Chemistry) defines SHE as follows: “The standard hydrogen electrode consists of a platinum electrode in contact with a solution of H^+ at unit activity and saturated with H_2 gas with a fugacity referred to the standard pressure of 10^5 Pa” [3]

2 Introduction to Electrochemical Energy Storage Devices

An electrochemical capacitor (alternatively called a supercapacitor or ultracapacitor) is a device in which a typically high surface area electrode material, based mostly on carbon, is charged so that an excess charge layer at the electrode surface is created,

and oppositely charged ions form a layer in solution, such that an EDL with an electrical potential difference between solution and electrode is the result [4–7]. Simultaneous diminution of the layers in the solution and at the electrode surface by release of ions and charge in the electrode results in a rapid release of electric charge and a repeal in the electrical potential difference [6, 8–13]. Electrode materials and electrolytes for electrochemical capacitors are reviewed in [13–17]. In contrast, batteries generate electrical energy by conversion of chemical energy via redox reactions taking place at the active materials, namely the negative and positive electrode in one or more electrically interconnected electrochemical cells. Batteries can be classified into primary (non-rechargeable) and secondary (rechargeable) batteries, depending on whether they are capable of being recharged by applying an electric current [18]. During discharge, each cell gives a current I_{dis} (A) at a voltage $V_{\text{dis}}(q)$ (V), which is dependent on the state of charge of the cell, up to a defined period of time t_{dis} (h). The current flow over time is defined as the discharge capacity (Q_{dis})

$$Q_{\text{dis}} = \int_0^{t_{\text{dis}}} I_{\text{dis}} dt. \quad (1)$$

This can be referred to by unit volume, as the volumetric discharge capacity (Ah L^{-1}), or by unit weight, as the specific discharge capacity (Ah kg^{-1}) [19]. The (relativized) theoretical specific capacity q_{th} of a given electrode material depends on the number of electrons exchanged, z , and its molecular or atomic weight M (g mol^{-1}). F is the Faraday constant ($96,485 \text{ As mol}^{-1}$).

$$q_{\text{th}} = \frac{zF}{M} \quad (2)$$

The specific discharge energy (E_{dis}) (Wh) supplied by any cell is determined by the discharge voltage $V_{\text{dis}}(Q)$ as well as the obtained absolute discharge capacity (Q_{dis})

$$E_{\text{dis}} = \int_0^{Q_{\text{dis}}} V_{\text{dis}}(Q) dQ. \quad (3)$$

Energy available per unit weight is called the specific energy (Wh kg^{-1} or mWh g^{-1}), also called gravimetric energy density. On the other hand, the amount of energy that is stored per unit volume is called the volumetric energy density (Wh L^{-1}), referred to simply as energy density in many reports [18–20].

The discharge power (P_{dis}) [specific power (W kg^{-1}) and volumetric power density (W L^{-1})] is determined by the discharge voltage V_{dis} as well as the discharge current I_{dis}

$$P_{\text{dis}} = V_{\text{dis}} I_{\text{dis}} = R_{\text{i}}(I_{\text{dis}})^2. \quad (4)$$

During discharge of the cell, an internal cell resistance (R_{i}) (Ω) reduces V_{dis} compared to the open-circuit voltage (V_{oc}) (V) by an overvoltage (η) (V). The magnitude of the overvoltage depends upon the value of the current drawn as well as the state

of charge of the cell [21]. The overvoltage consumes part of the energy as irreversible Joule heat (J)

$$\eta = R_i I_{\text{dis}}, \quad (5)$$

$$V_{\text{dis}} = V_{\text{oc}} - \eta(q, I_{\text{dis}}). \quad (6)$$

The thermodynamic value of the cell voltage under open circuit conditions is determined by the difference between the electrochemical potentials of the negative ($\tilde{\mu}_n$) and positive ($\tilde{\mu}_p$) electrode (J mol^{-1}) including the Faraday constant [19, 22, 23]; which can also be expressed as the difference in standard electrode potential of positive (E_p^0) and negative (E_n^0) electrode: [21, 24]

$$V_{\text{oc}} = \left| \frac{\tilde{\mu}_n - \tilde{\mu}_p}{F} \right| = E_p^0 - E_n^0 \quad (7)$$

The standard electrode potential of an electrochemical reaction is commonly reported with respect to the standard hydrogen electrode (SHE) as shown in Table 1.

The first primary cell, the voltaic pile, was developed by Volta between 1790 and 1800. It was made of elements based on copper disc/brine-soaked cardboard/zinc disc connected in series. Only 2 years later, Ritter built the first accumulator, by replacing the zinc discs in the voltaic pile by copper plates [26]. The first commercially successful rechargeable battery was the lead acid battery developed by Planté in 1859. The lead acid battery uses lead oxide as the positive electrode material,

Table 1 Standard electrode potential values of common battery materials in volts relative to the standard hydrogen electrode (SHE)^a

Half cell reaction	E°/V
$\text{Li}^+(\text{aq}) + \text{e}^- \leftrightarrow \text{Li}(\text{s})$	- 3.01
$\text{Li}^+(\text{aq}) + \text{C}_6(\text{s}) + \text{e}^- \leftrightarrow \text{LiC}_6(\text{s})$	- 2.9
$\text{Na}^+(\text{aq}) + \text{e}^- \leftrightarrow \text{Na}(\text{s})$	- 2.71
$\text{Mg}^{2+}(\text{aq}) + 2\text{e}^- \leftrightarrow \text{Mg}(\text{s})$	- 2.38
$\text{Cd}(\text{OH})_2(\text{s}) + 2\text{e}^- \leftrightarrow \text{Cd}(\text{s}) + 2\text{OH}^-(\text{aq})$	- 0.81
$\text{Zn}^{2+} + 2\text{e}^- \leftrightarrow \text{Zn}(\text{s})$	- 0.76
$\text{PbSO}_4(\text{s}) + 2\text{e}^- \leftrightarrow \text{Pb}(\text{s}) + \text{SO}_4^{2-}(\text{aq})$	- 0.36
$2\text{H}^+ + 2\text{e}^- \leftrightarrow \text{H}_2(\text{g})$	0
$\text{Cu}^{2+} + 2\text{e}^- \leftrightarrow \text{Cu}(\text{s})$	+ 0.34
$\text{Ag}_2\text{O}(\text{s}) + \text{H}_2\text{O} + 2\text{e}^- \leftrightarrow 2\text{Ag}(\text{s}) + 2\text{OH}^-$	+ 0.35
$\text{NiOOH} + \text{H}_2\text{O} + \text{e}^- \leftrightarrow \text{Ni}(\text{OH})_2 + \text{OH}^-(\text{aq})$	+ 0.45
$\text{Br}_2(\text{aq}) + 2\text{e}^- \leftrightarrow 2\text{Br}^-(\text{aq})$	+ 1.08
$\text{Cl}_2(\text{g}) + 2\text{e}^- \leftrightarrow 2\text{Cl}^-(\text{aq})$	+ 1.36
$\text{PbO}_2(\text{s}) + \text{SO}_4^{2-}(\text{aq}) + 4\text{H}^+ + 2\text{e}^- \leftrightarrow \text{PbSO}_4(\text{s}) + 2\text{H}_2\text{O}$	+ 1.69

^aData taken from [25]

metallic lead as the negative electrode material and aqueous sulfuric acid as electrolyte. Practical lead acid batteries have a nominal voltage of 2 V and a specific energy of $\approx 35 \text{ Wh kg}^{-1}$ [25]. Even today, the lead acid battery powers numerous battery applications. The need for higher energy storage systems for advanced applications led to the development of nickel/cadmium (NiCd), nickel/metal hydride (NiMH) (both using aqueous KOH as electrolyte and having a nominal cell voltage of 1.2 V) and lithium ion batteries (LIBs) [25]. Detailed information on the aqueous battery systems lead acid, NiCd and NiMH is given in [18, 25]. Today, together with the lead acid battery, the LIB is the most important rechargeable battery technology, with double-digit compound annual growth rates. The liquid electrolyte in LIBs requires moving away from aqueous media, since water-based electrolytes have a too narrow electrochemical stability window regarding the operation voltage range of LIBs [27]. The use of aprotic liquid organic electrolytes adds some complexity to the picture, since electrochemistry and ion transport properties in these media are much less studied. Furthermore, due to the sensitivity to hydrolysis of certain cell components, in particular the electrolyte, LIBs have to be assembled in a dry atmosphere [28]. Further LIB technologies, such as Li/air [29–31], Li/S [29, 32, 33], Na-ion [34], Mg metal [35, 36], Ca metal [37, 38], Al metal [38–40], dual-ion [41–44] as well as lithium metal batteries, dual-ion batteries and LIBs based on organic electrode materials [45, 46] are still in the research and development stage and are detailed in the stated literature and in [47]. They are not discussed in the frame of this review.

3 Introduction to Lithium Ion Cell Chemistry

Due to their flexibility in terms of cell chemistry, electrode (micro-) structure and design, LIBs can be constructed to meet a broad range of power to energy ratios (P/E), thus making them a most suitable battery technology for application in all kinds of electric vehicles with different P/E ratios, such as hybrid (HEV, $P/E \approx 15$), plug-in hybrid (PHEV, $P/E \approx 8$) and fully battery electric (BEV, $P/E \approx 3$) [49]. In general, LIBs comprise a negative and positive electrode capable of Li^+ ion insertion/de-insertion, and a separator that is soaked with a lithium salt containing mixture of liquid organic solvents to ensure the rapid transfer of Li^+ ions within the cell [50, 51]. The separator, a porous polyolefin membrane with a thickness of 15–25 μm , acts as an electronic insulator and prevents direct electronic contact between the two electrodes. The electrode active materials, embedded in a mixture of conductive additive [52, 53] and binder [54], are coated on current collectors, where Cu foil (8–18 μm) is preferably used for the negative electrode [55] and Al foil (12–20 μm) for the positive electrode [46–59]. Figure 1 depicts a typical wound cell assembly with double-side-coated porous positive electrode, double-side-coated porous negative electrode separated by an inner and outer separator.

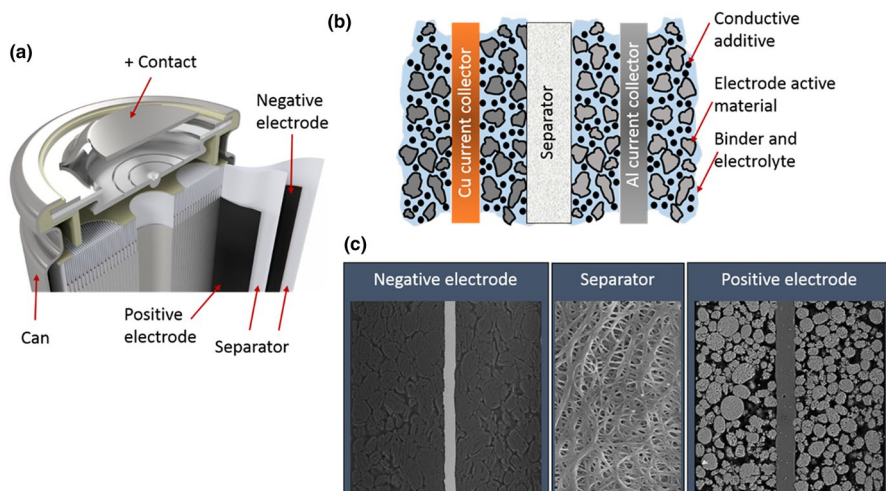
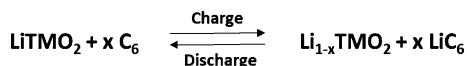


Fig. 1 **a** Wound cell construction including negative and positive electrode, as well as inner and outer separator. **b** Double-side-coated negative and positive composite electrodes. **c** Scanning electron micrograph (SEM) top view on separator and SEM cross sections of double-side-coated positive and negative composite electrodes

During charging of a LIB, reduction takes place at the negative electrode. Thereby, the negative electrode is forced to accommodate electrons from the positive electrode, which flow through the external current circuit. Simultaneously, the negative electrode inserts Li^+ ions, which are extracted at the positive electrode side into the solution phase and migrate and diffuse through the bulk electrolyte to the negative electrode side, to ensure the charge balance. As a result, the positive electrode active material is oxidized. In the case of the discharge process, the redox reactions are inverted. During the discharge process, the negative electrode acts as anode and the positive electrode as cathode. As seen in the overall reaction of the LIB depicted in Scheme 1, the active Li^+ ions are shuttled between two insertion host electrodes during charge and discharge of the LIB.

The electrochemical role of both electrodes changes between anode and cathode, depending on the direction of the current flow through the cell. However, throughout the literature and in the remainder of this manuscript, the positive electrode is named as the cathode and the negative electrode as the anode.



Scheme 1 Overall cell reaction during charge and discharge of a lithium ion battery (LIB) based on graphite as negative electrode active material and lithium transition metal oxide (TM = Mn, Co, Ni, etc.) as positive electrode active material

4 Anode Materials for LIBs

4.1 Lithium Metal, the Ancestor Anode of LIB Electrodes

Metallic Li is regarded as the most promising anode material for high energy density Li-based batteries, due to its outstanding properties. Among all metals, the Li/Li⁺ redox couple has the lowest potential value (Table 1) and Li has the lightest weight, resulting in a low operation potential and a high specific capacity of Li metal anodes, respectively. However, the use of Li metal electrodes comes with serious safety issues upon repetitive charge and discharge of the cell, originating from extensive shape changes, inhomogeneous Li deposition and formation of high surface area Li, commonly referred as Li dendrites in the literature, when liquid organic solvent-based electrolytes are used [60–62]. In the worst case scenario, Li dendrites grow through the separator and locally short-circuit the cell [63]. Lithium metal polymer batteries, comprising a dry solid polymer electrolyte and a LiFePO₄ cathode are already a practically used reality (Fig. 2). Specific ionic liquid-based electrolytes, also in composites with polymers, enable the use of the metallic Li electrode [64].

4.2 Classification of Anode Materials

As metallic Li is still a safety concern when used in the rechargeable mode, anode materials based on Li⁺ ion uptake have been pursued for LIBs. The materials can be classified into the following categories according to their type of reaction with the Li⁺ ion: insertion, alloying and conversion reactions (Fig. 3) [66]. Many metals can form alloys or intermetallic phases with Li; however, most of the literature is

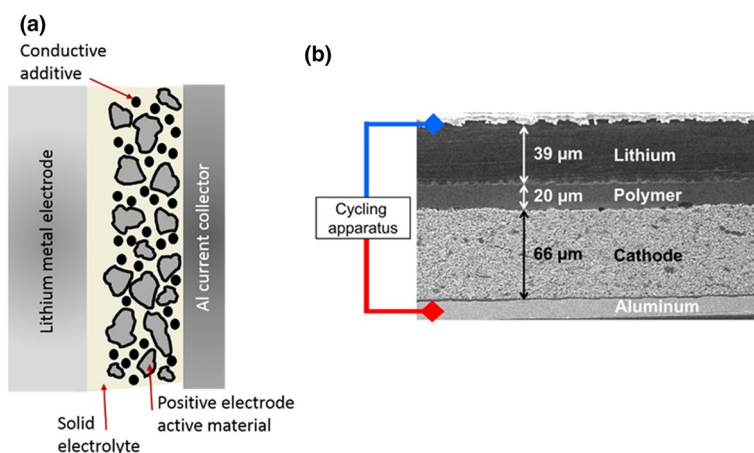


Fig. 2 **a** Schematic illustration of a lithium metal polymer battery. **b** Cross-section SEM image of the cell. Adapted with permission from [65]. Copyright (2015) American Chemical Society

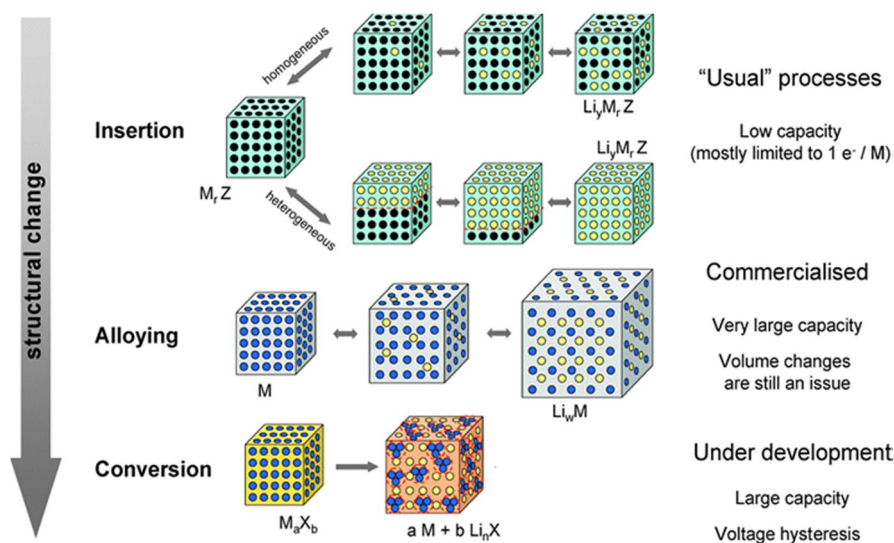


Fig. 3 A schematic representation of the different reaction mechanisms observed in electrode materials for lithium-based batteries. *Black circles* Voids in the crystal structure, *blue circles* metal, *yellow circles* lithium. Reprinted with permission from [28]. Copyright (2009) Royal Society of Chemistry

devoted to Si [67] and Sn-based [51, 68] anode materials [51, 69–72]. Still, the main challenge arising with the use of Si, Sn (and other Li storage metals) as negative electrode active material is the severe volume change (up to 400%) that the Li storage metals experiences during Li^+ ion uptake and release, thus leading to particle cracking and disintegration of the electrode structure [67]. Various approaches to overcome the challenges arising with the Li storage metal volume change have been reported, with the use of active-inactive composites (e.g., Si–C composites) as the most prominent ones. Si–C composite electrodes with Si content in a low single-digit range have already been commercialized. Recent research progress in so-called conversion reaction-based anodes has been reviewed in [73, 74]. The large voltage hysteresis in conversion materials is still a major obstacle leading to a low energy efficiency of these materials during charge and subsequent discharge [20, 75]. For this reason, conversion anodes are used only at a laboratory scale and will have no tangible effect on the LIB cell chemistry in the next years. Commercial LIBs use mainly insertion anode materials, such as graphite, hard carbon or lithium titanate ($\text{Li}_4\text{Ti}_5\text{O}_{12}$, LTO).

4.3 Graphitic and Non-Graphitic Carbon Anodes

Carbon materials can be classified into graphitic (materials having a layered structure characterized by crystalline domains) and non-graphitic (disordered structure, characterized by amorphous domains). Depending on their ability to develop a graphite structure during heat treatment, non-graphitic carbons can be further

divided into graphitizing carbons (referred as soft carbons) and non-graphitizing carbons (referred as hard carbons) [51, 76]. Each type of carbon has its own current and potential characteristics of the Li^+ ion intercalation/de-intercalation reaction. Graphitic carbons comprise stacked graphene layers in the stacking sequence AB (hexagonal graphite) or ABC (rhombohedral graphite), which are held together by weak van der Waal forces [77]. During electrochemically induced lithiation, a maximum content of one Li^+ ion per six carbon host atoms can be stored, corresponding to a theoretical specific capacity of 372 mAh g^{-1} . The process of Li^+ ion insertion proceeds via the prismatic surface, and is accompanied by a change in the graphite stacking sequence to AA, thus leading to a change of the graphene interlayer distance of $\approx 10\%$. Thereby, Li^+ ion insertion proceeds via a staging mechanism in which the Li^+ ion fully intercalates into very distant graphene layer gaps before occupying the space between neighboring layers. The staging process is characterized by well-defined potential plateaus in the potential region between ≈ 0.25 and $0.05 \text{ V vs. Li/Li}^+$ (Fig. 4) [51].

The plateaus arising in the potential profile are due to the coexistence of two phases (P) according to Gibbs phase rule.

$$\mathcal{F} = C - P + 2 \quad (8)$$

The number of degrees of freedom (\mathcal{F}) is given by the number of components (C) present and the number of coexisting phases present. In the case of Li^+ ion intercalation into graphite, there are two components, viz., the Li^+ ion and the graphite host structure, as well as two coexisting phases. This means that if the values of two intensive thermodynamic parameters, such as temperature and pressure, are specified, no \mathcal{F} are left. Thus, there is no independent \mathcal{F} , which means that the electrochemical potential is constant over the lithiation degree (plateau region in the potential profile) in the specific two-phase region. More information on the Gibbs phase rule and its application in batteries can be found in [78]. Due to the low operation potential of graphite anodes, all known liquid aprotic electrolytes are

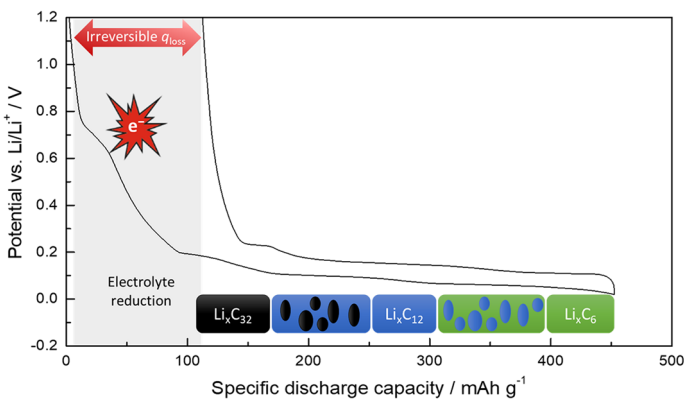


Fig. 4 The potential profile of graphite has several stages distinguished as a result of single and two-phase regions

thermodynamically unstable at the anode/electrolyte interface. However, the charge-consuming reduction (irreversible q_{loss} in Fig. 4) of the commonly used lithium hexafluorophosphate (LiPF_6)/organic carbonate-based electrolyte in the initial charge/discharge cycles, especially during the first charge of the cell, leads to the formation of a passivation layer, the well-known solid electrolyte interphase (SEI) [63], and thus to kinetic stability. In this regard, the electrolyte components with the lowest reductive stability react first [79]. In particular, Baluena et al. studied the reduction stability of solvents by means of computational chemistry and pointed out the importance of Li^+ ion–solvent coordination for predicting stability limits [80, 81]. Film formation is related to the surface properties of the carbon/graphite material [82, 83] and the electrolyte composition used [84–86], and is associated with the irreversible capacity loss and electrolyte depletion. For detailed information on carbon anodes, the reader is referred to [79, 87].

4.4 Lithium Titanate

Lithium titanate spinel ($\text{Li}_4\text{Ti}_5\text{O}_{12}$, LTO) is an alternative commercialized anode material, known for its long cycle life and improved safety characteristics compared to graphite anodes, especially at low temperature applications and fast charge rates [88, 89]. On the one hand, this is due to the high Li^+ ion intercalation/de-intercalation potential of 1.55 V vs. Li/Li^+ , which is higher than most of the reduction onset potentials of common liquid aprotic electrolyte components. On the other hand, LTO undergoes nearly no volume change during Li^+ ion uptake and is therefore considered as zero-strain insertion material [66]. However, the increased safety performance comes along with a lower theoretical specific capacity of only 175 mAh g^{-1} , thus resulting in an overall low specific energy [25]. The recent development and application of LTO is reviewed in [90, 91].

5 Cathode Materials for Lithium Ion Batteries

To date, there is a wide range of materials for positive electrodes (cathodes), belonging either to the group of insertion materials or to conversion materials [49, 92]. In this review, only the most relevant commercialized cathode materials are discussed. For further detailed information on cathode materials under development, much more specialized reviews are available elsewhere [92–95]. Within the class of insertion materials, most of them (in the discharged state) can be expressed chemically as a crystal composed of Li^+ ions, transition metal (TM) cations and anions based on either -phosphates, -sulfides or -oxides (LiTMPO_4 , LiTMS_2 , $\text{Li}_x\text{TM}_y\text{O}_z$). Beyond the performance-related aspects, other features including high reversible specific capacity, high mean discharge potential and high rate capability, price, safety and toxicity need to be considered for selection as well. The classification of insertion cathode materials conventionally occurs according to the type of spatial Li^+ ion transport within the crystal structure, which is either one, two or three dimensional (1D, 2D, 3D), as depicted in Fig. 5.

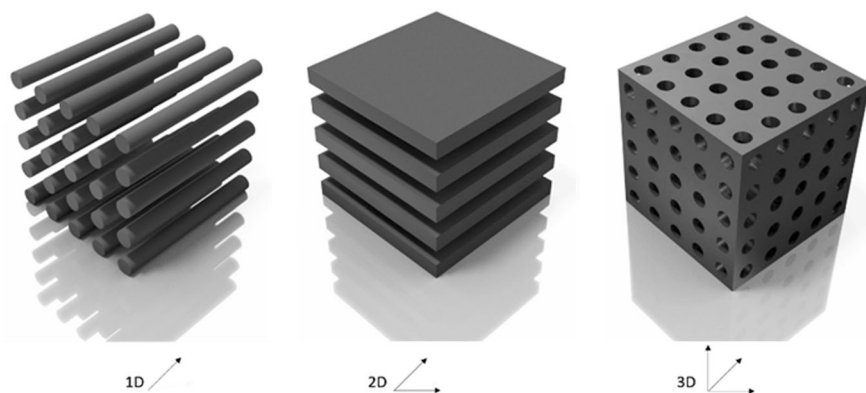


Fig. 5 Classifications of active materials with respect to the spatial Li^+ ion transport pathway within the crystal structure

LiTMPO_4 and LiTMS_2 -based electrodes belong to the 1D and the 2D family, respectively, revealing the olivine and layered crystal structure type. The $\text{Li}_x\text{TM}_y\text{O}_z$ -based electrodes can be subdivided into $\text{Li}_x\text{TM}_y\text{O}_2$ and $\text{Li}_x\text{TM}_y\text{O}_4$ electrodes, which belong to the 2D (layered crystal structure type) and 3D (spinel crystal structure type) families. While the mean potential of each crystal structure is tailorable by variation of TMs, the theoretical specific capacity is limited by the respective molar mass according to Eq. 2. Consequently, the highest theoretical specific capacities can be assigned to layered oxides, making them the most promising cathode material candidates up to date. For instance, the theoretical specific capacities for prominent representatives of each crystal structure, that are LiFePO_4 (LFP), LiTiS_2 (LTS), $\text{LiNi}_{1/3}\text{Mn}_{1/3}\text{Co}_{1/3}\text{O}_2$ (NMC111) and $\text{LiNi}_{0.5}\text{Mn}_{1.5}\text{O}_4$ (LNMO), amount to 170, 225, 278 and 148 mAh g^{-1} , respectively, which finally points to the superior role of the layered oxides in this regard. Even though, in practice, the specific capacity utilization in layered oxides must be restricted for reversibility reasons, as the delithiation beyond a respective threshold value is accompanied by thermodynamic structural instabilities [96], layered oxides have dominated the LIB market in past decades [57, 97]. Because there is still large scope for specific energy improvement, research and development efforts for layered oxides are still intense.

Generally, the characteristic layered oxide reactions upon delithiation (charge) and lithiation (discharge) are accompanied by a continuous increase and decrease of the electrode potential, as depicted in Fig. 6 using the example of NMC111 active material.

Hence, the targeted goal of specific energy increase can be realized simply by the increase of the cathode charge potential. This would increase not only the discharge potential (U_{dis}) (V), but also the specific discharge capacity (q_{dis}), which both contribute to the increase in specific discharge energy according to Eq. 3 [98, 99]. However, these benefits are accompanied with a continuous increase in specific capacity loss (q_{loss}), when a certain potential threshold value is exceeded. The increase of q_{loss} is closely intertwined with undesired consequences with respect to cycle life

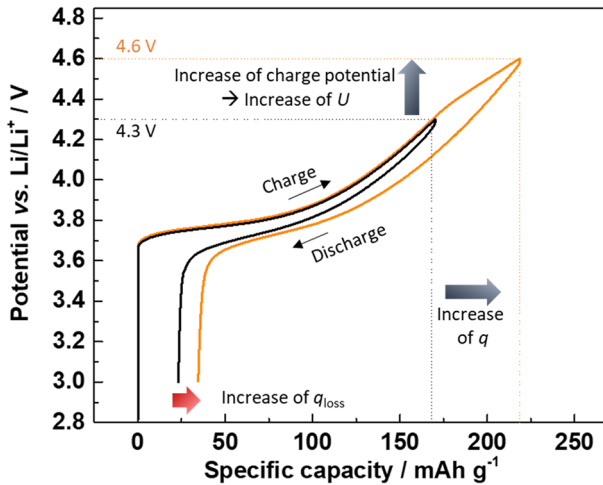
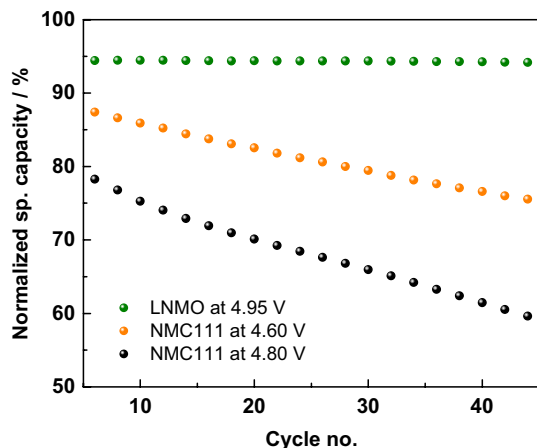


Fig. 6 Initial charge/discharge potential curve as a function of the specific capacity of NMC111, exemplary representing a layered oxide. The increase of the charge potential would increase the specific capacity (q), but also the specific capacity loss (q_{loss})

and safety aspects. Recent studies revealed that the origin of q_{loss} increase could be attributed predominately to structural intrinsic changes of the active material, leading finally to an impeded and incomplete lithiation during discharge [96, 100]. Furthermore, it could be pointed out that the specific capacity fade (limiting the cycle life) is dependent on the type of active material rather than solely the charge potential [101]. The exemplary comparison of the specific capacity fade of LNMO and NMC111 electrodes in Fig. 7 demonstrates that, despite a higher charge potential (4.95 V vs. Li/Li⁺ for LNMO) the specific capacity fade is even less than for the NMC111 electrode having lower charge potentials. For the same active material though, the specific capacity fade increases with the charge potential, which could

Fig. 7 Charge/discharge cycling with normalized specific discharge capacities for LNMO/Li (charged to 4.95 V vs. Li/Li⁺) and NMC111/Li (charged to 4.60 V and 4.80 V vs. Li/Li⁺) half cells after formation. Data reevaluated from [102]



be attributed to increased structural instabilities associated with increased delithiation amounts, as pointed out in Fig. 6.

Consequently, the key to the desired performance improvement is intertwined with improvements in the active material itself. Therefore, the relation between chemical composition, structure and properties needs to be characterized and understood. From a crystallographic point of view, the layered oxides are based on alternating TM and Li^+ ion layers, each residing in oxygen octahedral coordinated 3a and 3b sites, respectively (Fig. 8). Properties with respect to performance and stability of layered oxide-based active materials can be tailored via (1) coating of the active material surface and/or (2) variation of the TMs, which are based conventionally on Ni, Co and Mn including doping with other elements, and/or (3) overlithiating of the material leading to $\text{Li}_{1+x}\text{TM}_{1-x}\text{O}_2$ type layered oxides.

(1) The advantage of active material coating is associated with stabilization of the electrode/electrolyte interface towards parasitic side reactions and increasing thermal and electrochemical stability [103–105]. However, the implementation of inactive or less active mass through coating not only decreases the gravimetric energy density but also results in an additional resistance for Li^+ ion migration, which needs to be outweighed prior to application. (2) Layered oxides can be composed of single or even mixtures of TMs enabling a wide range of possible combinations. A prominent, already commercialized, single TM-based active material is LiCoO_2 (LCO), showing good electrochemical performance for capacity utilizations up to $\approx 50\%$ of theoretical capacity. Exceeding this limit (e.g., in case of overcharge) leads to safety hazards, which are associated with O_2 release attributable to chemical instability

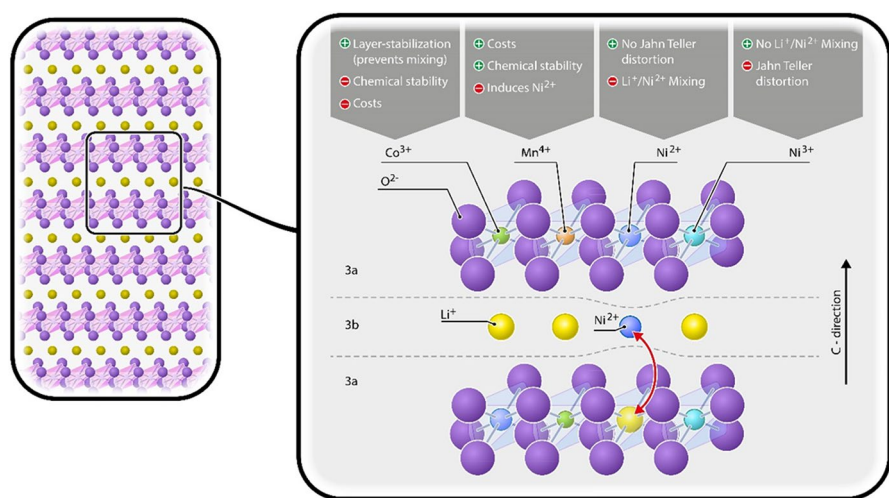


Fig. 8 Left Crystal structure of layered oxide-based cathodes, revealing altering layers of Li^+ (yellow bullets) and transition metals (TMs; coordinated within violet octahedra). Right Magnification including two TM layers and a Li^+ layer. The oxygen (violet bullets) coordinated TMs reside in Wyckoff 3a sites, while the analogues coordinated Li^+ resides in Wyckoff 3b sites. The $\text{Li}^+/\text{Ni}^{2+}$ mixing phenomenon is marked with a red double arrow. The pros and cons of each possible TM within layered oxide-based cathodes are highlighted. Reprinted with permission from [101]. Copyright (2017) John Wiley and Sons

of LCO [106]. The specific capacity restrictions, safety issues, toxicity, costs and resource problem of Co have necessitated the search for alternative active materials [107]. The substitution of Co with Ni, yielding LiNiO₂ (LNO), indeed enables a higher capacity utilization, as the Ni-based layered oxide is thought to be more chemically stable (less risk of oxygen release). However, the cycle life and electrochemical performance, especially at elevated rates, do not meet the requirements necessary for application in LIBs. On the one hand, this is associated with the Ni³⁺ suffering from structural distortions due to the Jahn–Teller effect [108]. On the other hand, the synthesis yields non-stoichiometric Li_{1-x}Ni_{1+x}O₂ compounds, resulting in Ni²⁺ ions placed within the Li⁺ ion layer, mitigating Li⁺ ion mobility within the Li⁺ ion layer for several reasons: (1) They act as obstacles interfering the Li⁺ ion migration path, due to increased electrostatic repulsion between Ni²⁺ and Li⁺ ions.

(2) They decrease the slab space (*c*-direction) within the Li⁺ ion layer due to higher valence of Ni²⁺ ions compared to Li⁺ ions [95]. Partial substitution of Ni with Co and Al effectively reduces the cationic disorder and improves the thermal as well as electrochemical performance. The paradigm mixture LiNi_{0.8}Co_{0.15}Al_{0.05}O₂ (NCA) is a commercial material, which is used, for example, in Panasonic wound cells for Tesla BEVs [92]. With respect to cost issues and chemical stability, LiMnO₂-based layered oxides were also considered for application in LIBs [109]. However, this material suffers from poor cycle life due to Jahn–Teller effect related structural instabilities and irreversible phase transformations attributable to its trivalent state (Mn³⁺) [110]. Interestingly, the tetravalent Mn (Mn⁴⁺) has a beneficial effect with respect to structural and thermal stability [109, 111]. However, as the average TM oxidation state within the LiTMO₂ structure is TM³⁺, the desired Mn⁴⁺ can be realized only in combination with (at least) equal amounts of Ni²⁺. These valence states are obtained according to crystal field theory, when Mn³⁺ and Ni³⁺ are originally incorporated within the structure [112]. However, the associated Ni²⁺ is undesired, because its similar ionic radius to Li⁺ (69 vs. 76 pm) leads to a partial Li⁺/Ni²⁺ site exchange, known as Li⁺/Ni²⁺ mixing. This phenomenon, depicted in Fig. 8 (red arrow), leads to the presence of Ni²⁺ within the Li⁺ ion layer, leading to the undesired effects described above for LNO active material [113]. Interestingly, the implementation of Co³⁺, yielding the well-known LiNi_xMn_yCo_zO₂ (NMC; *x* + *y* + *z* = 1) family, suppresses the Li⁺/Ni²⁺ mixing extent, but at the expense of the disadvantages of the Co element [114, 115]. The pros and cons of the three individual TM are summarized in Fig. 8, pointing out the required optimized trade-off between electrochemical performance, structural stability and cost as well as cycle life [107].

(3) The overlithiation of the active material occurs at the cost of the amount of redox-active TM within the structure, which is consequently accompanied with a decrease in theoretical specific capacity. As the theoretical specific capacity is not utilized completely during LIB operation, overlithiation has its advantage in increasing the TMs average oxidation state. As pointed out above, the lower oxidation states of Ni (Ni²⁺) as well as Mn (Mn³⁺) cause severe performance disadvantages, which can be minimized by increasing the overlithiation degree. Besides this advantage of conventional LiTMO₂ chemistry, overlithiated materials also reveal an uncommon chemistry, enabling specific capacities even higher than theoretical values. The

extra specific capacity in those materials is thought to originate from oxidation of the oxygen within the structure. Even though the specific capacity for this structure is remarkable, the reversibility upon charge/discharge cycling remains a big challenge [116, 117].

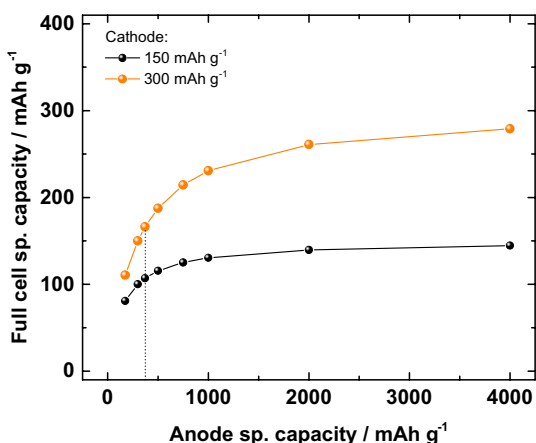
It is worth noting that, to date, the specific capacity bottleneck within a full cell setup is the positive electrode (cathode). Further improvements in specific capacities of the negative electrode (anode) are not significantly beneficial as long as the specific capacity of the cathode remains constant [47]. For reasons of simplicity, focusing only on the masses of the active materials for both cathode and anode, this correlation was calculated as depicted in Fig. 9.

The increase of the specific capacity of the anode within a full cell approaches the specific capacity value of the cell-capacity-limiting electrode, i.e. the cathode, asymptotically. Improvements in specific anode capacity are noticeable only up to a certain point ($\approx 1000 \text{ mAh g}^{-1}$). For sure, it is still reasonable to focus on the anode, as graphite, as the state-of-the-art (SOTA) anode material, reaches a specific capacity of just 372 mAh g^{-1} (dashed line). However, the specific capacity improvement of the cell-capacity-limiting electrode, the cathode, would have a very beneficial impact on the overall specific full cell capacity, which points to the importance of exploratory research and development in this field [118]. Ab initio computational modeling allows for prediction of the influence of different TMs and doping elements on the Li^+ ion diffusion kinetics, thus guiding more effective experimental research [119].

6 Electrolytes for LIBs

The ability to conduct ions, and in particular Li^+ ions, is the main function of the electrolyte in LIBs. Within the LIB, the electrolyte belongs to the inactive materials; however, its effect on the chemical nature and morphology of the formed interphases at the electrode/electrolyte interfaces have a major influence on the cycle life, power capability

Fig. 9 Full cell specific capacities as a function of the anode-specific capacities for constantly held cathode-specific capacities of 150 and 300 mAh g^{-1} . Dashed line Specific capacity of graphite anode material of 372 mAh g^{-1} . For the calculation only the masses of the active materials are considered

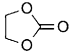
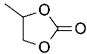
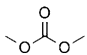
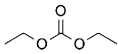
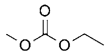


and safety performance of the LIB. Research on electrolytes for lithium-based batteries can be grouped into ceramic solid electrolytes [120], polymeric electrolytes [121, 122], ionic liquid based electrolytes [123, 124], liquid organic electrolytes [125–128], liquid aqueous electrolytes [129], as well as hybrid electrolytes [64, 130]. However, most of the electrolytes used in commercial LIBs are liquid organic solvent-based electrolytes, comprising a Li salt dissolved in a blend of aprotic organic solvents. Surprisingly, as compared to research outcome devoted to cathode cell chemistries, advances in electrolyte research and development have been scarce over the past 25 years [127]. The LIB commercialized by Sony in 1991 comprised a LCO positive electrode, a non-graphitizing carbon negative electrode and LiPF_6 dissolved in a mixture of propylene carbonate (PC) and diethyl carbonate (DEC) as electrolyte [131]. With the energetic advantage of highly graphitic carbon being used as negative electrode in LIBs, ethylene carbonate (EC) replaced PC and became an indispensable component of every electrolyte formulation [125]. The structures of aforementioned organic carbonates are presented in Table 2. Since then, the skeleton electrolyte based on LiPF_6 in a mixture of EC and linear alkyl carbonates has not changed significantly. In liquid electrolytes, the ionic conductivity (κ) ($\Omega^{-1} \text{ cm}^{-1}$) is determined by the ion concentration (c_i) (mol L^{-1}) and the ion mobility (u_i) ($\text{m s}^{-1} \text{ V}^{-1}$) [132]

$$\kappa = \sum_i |z_i| F c_i u_i, \quad (9)$$

$$u_i = \frac{|z_i| e_0}{6\pi\eta r_i}. \quad (10)$$

Table 2 Melting point (T_m), boiling point (T_b), flash point (T_f), viscosity (η) and relative permittivity (ϵ_r) and of commonly used organic carbonate solvents, viz. ethylene carbonate (EC), propylene carbonate (PC), dimethyl carbonate (DMC), diethyl carbonate (DEC) and ethyl methyl carbonate (EMC)^a

Solvent	Structure	$T_m/^\circ\text{C}$	$T_b/^\circ\text{C}$	$T_f/^\circ\text{C}$	$\eta/\text{mPa s}^{-1}$ (at 25 °C)	ϵ_r (at 25 °C)
EC		36	238	143	1.90 (40 °C)	90 (40 °C)
PC		-49	242	138	2.50	65
DMC		5	90	17	0.59	3.1
DEC		-74	127	25	0.75	2.8
EMC		-53	108	23	0.65	3.0

^aData taken from [126]

Here, z_i is the charge of the ion I, e_0 is the unit charge ($1.602 \cdot 10^{-19}$ C), η is the temperature dependent dynamic viscosity of the solvent ($\text{kg s}^{-1} \text{m}^{-1}$) and r_i is the stokes radius (radius of the ion I including its solvation sphere) (m) [132]. Molecular dynamics simulation are a suitable tool to study Li^+ ion coordination by the solvent molecules and the Li^+ -anion ion pair formation [133, 134], and can be considered as complementary method to the spectroscopic methods, such as Raman and NMR, to study the structure of the ion solvation shell [135]. In LiPF_6 -based electrolytes, solvated Li^+ ions have a lower mobility than the less solvated PF_6^- ions, thus resulting in the transference number of Li^+ ion in the range of 0.2–0.4 [125]. The transference number (t_i) is the fraction of the total current that is transferred by a particular ion:

$$t_i = \frac{|I_i|}{\sum_i |I_i|} \quad (11)$$

In this regard, it is important to remember that the power performance of the LIB is determined only by the current carried by the Li^+ ion. Furthermore, a low Li^+ ion transference number leads at the same time to an increased anion movement and enrichment at the electrodes, causing concentration polarization [125]. Equation 9 is valid only for electrolyte salts that dissociate completely into fully solvated ions. However, with decrease of the relative permittivity (ϵ_r) of the used electrolyte solvents, complete dissociation can no longer be achieved. Part of the dissolved electrolyte salt remains undissociated, thus being present as contact ion pairs in the solution (Fig. 10).

Since contact ion pairs are macroscopically neutral species, they do not contribute to the total conductivity of the electrolyte. In general, in electrolyte solvents having $\epsilon_r < 10$, the amount of electrolyte salt that is dissociated into fully solvated ions is small except in very dilute solutions [132]. Whereas in electrolyte solvents with

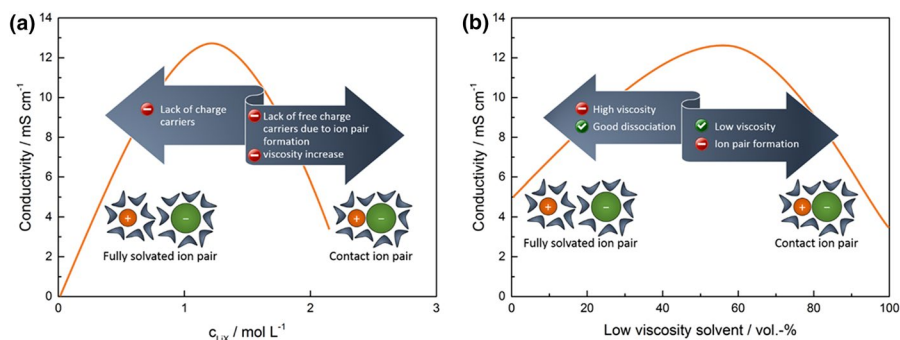


Fig. 10 **a** Conductivity change as a function of increasing electrolyte salt concentration. **b** Conductivity change of a 1 M LiPF_6 salt in a high relative permittivity solvent, such as ethylene carbonate (EC), as a function of increasing low viscosity solvent concentration, e.g., dimethyl carbonate (DMC). Redrawn from [47, 136]

$\epsilon_r > 40$, the fraction of electrolyte salt that forms contact ion pairs is small except in highly concentrated solutions [132]. Next to a high ϵ_r value, suitable solvent molecules need to have a low viscosity (η), according to Eqs. 9 and 10. Since solvents kinetically stable with Li combine either high viscosity and high relative permittivity or low viscosity and low relative permittivity, a solvent mixture, usually comprising solvents with high ϵ_r values and solvents with low η values, is used (Table 2). In almost all cases, electrolyte conductivity in mixed solvents is superior to that in single solvent-based electrolytes [125]. Semi-empirical quantum-mechanical (SQM) and density functional theory (DFT)-based COSMOtherm calculations can be used to estimate the melting/flash/boiling points, electrochemical stabilities and viscosities of electrolyte solvents [137, 138] and thus are very helpful for the preselection of suitable electrolyte components.

However, performance deterioration and safety risks caused by the poor thermal and chemical stability of present liquid aprotic electrolytes limit their application in LIBs to operation temperatures < 50 °C [139]. While reactions at the graphite/electrolyte interface have been studied intensively, the degradation reactions inside the bulk electrolyte induced by high voltage and high temperature, as well as the influence of the formed electrolyte decomposition products on battery safety and performance have been rarely discussed [139, 140]. Figure 11 shows the decomposition reaction of LiPF_6 in the presence of protic impurities resulting in the formation of various organophosphates [141–143]. However, the hydrolysis of LiPF_6 /organic

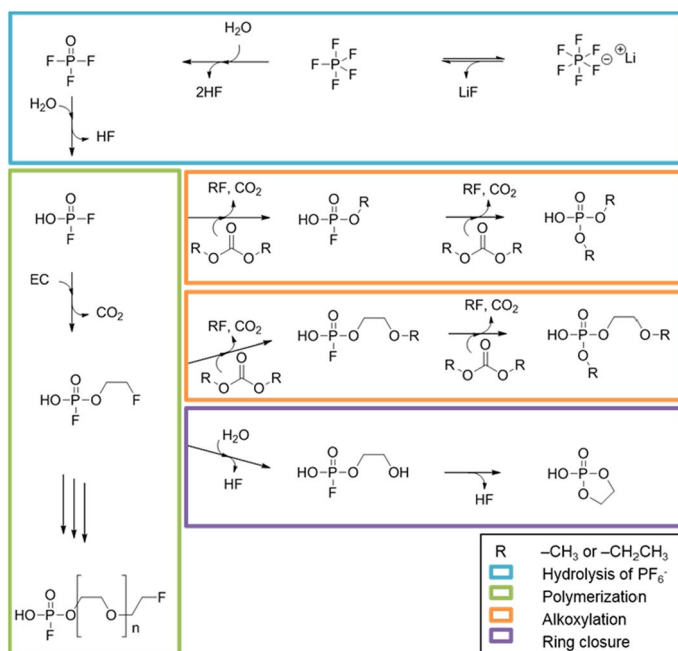


Fig. 11 Proposed decomposition mechanism of LiPF_6 . Reprinted with permission from [144]. Copyright (2015) Elsevier

carbonate-based electrolytes is still not fully understood, and support from computational chemistry is rare [103, 139, 141].

According to Eq. 7, the thermodynamic cell voltage of a LIB is determined by the difference between the electrochemical potentials of the anode and cathode. When the graphite anode is used with conventional LiPF_6 /organic carbonate-based electrolyte, the value of the graphite electrochemical potential lies well above the energy level value of the lowest unoccupied molecular orbital (LUMO) of the electrolyte. Because of the thermodynamic instability at the graphite/electrolyte interface, the electrolyte is reduced, which describes the electron transfer (ET) from the graphite electrode to the LUMO of the electrolyte. The reduction proceeds unless a passivation layer, the well-known SEI [63, 145, 146], is formed and prevents ET, or at least dramatically slows it down, as shown schematically in Fig. 12. The SEI is ideally considered as an electronic insulator and at the same time selectively permeable for only Li^+ ions [63]. Theoretically, a 5 V cathode material with an electrochemical potential lower than the energy level value of the electrolytes highest occupied molecular orbital (HOMO) leads to oxidation of the conventional LiPF_6 /organic carbonate-based electrolyte. ET from the HOMO of the electrolyte to the cathode takes place unless an effective passivation layer is formed. In this regard, it has been reported that the general trends obtained from DFT-calculated HOMO energies and computed oxidative stability limits often correlate with the experimental oxidation potentials of anions [147, 148] and solvents [149–151]. The lower the HOMO energy level of the solvent, the more stable is this compound toward oxidation. However, computed stability limits of investigated compounds are often significantly higher than experimentally measured values [152], where recent results even point to oxidative stabilities >5 V vs. Li/Li^+ of conventional electrolytes [153]. In this regard, it is important to consider the presence of solvent–solvent or solvent–ion complexes in the electrolyte, which can lead to significantly different

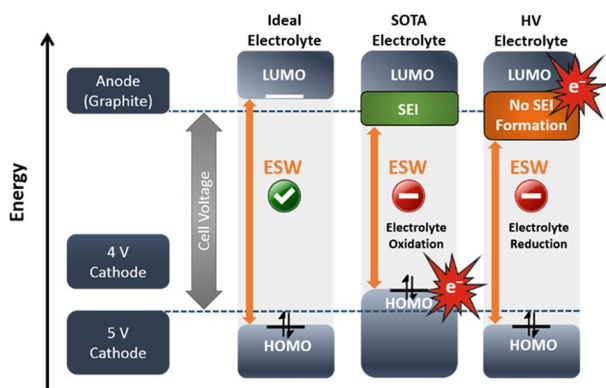
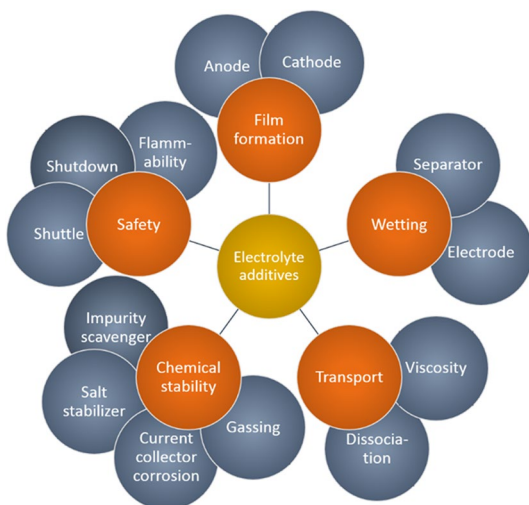


Fig. 12 Schematic energy diagram of a lithium ion battery (LIB) comprising graphite, 4 and 5 V cathode materials as well as an ideal thermodynamically stable electrolyte, a state-of-the-art (SOTA) LiPF_6 /organic carbonate-based electrolyte and a high voltage (HV) thermodynamically stable electrolyte. The electrochemical stability window (ESW), the lowest unoccupied molecular orbital (LUMO) energy level and highest occupied molecular orbital (HOMO) energy level are shown

electrochemical stability values compared to computing on isolated molecules [139, 154]. The LUMO energy level can be used to predict the reductive stability of the solvent [85, 155]. An understanding of electrochemical decomposition reactions is also important as it provides basic insights into the reactions and products involved in the formation of the electrode/electrolyte interphases [156, 157]. The calculation of oxidation and reduction potentials of electrolyte components serves to establish trends that can guide the selection of advanced electrolyte formulations [158]. Recent progress in research on high voltage stable electrolytes is reviewed in [159]. The most promising alternative solvent classes with increased oxidative stabilities are fluorinated carbonates [160–162], sulfones [149, 163], and aliphatic dinitriles [164, 165]. However, the high cost of production and poor compatibility with graphite anodes limit their applicability in LIBs. Today, nitriles are used only as co-solvents up to 10 vol% in commercial LIB electrolytes [159].

The use of electrolyte additives is one of the most economic and effective methods with which to tailor the performance of LIB with regard to desired functionality [166]. In general, the amount of an electrolyte additive is $\approx 5\%$ either by weight or by volume in order not to change the bulk electrolyte properties [166]. Hundreds of different additives have been reported in the literature and can be classified according to their functionality (Fig. 13). Vinylene carbonate (VC) is by far the most widely used and intensively studied film-forming electrolyte additive for graphite-based anodes [125, 127]. A small amount of VC (in most cases 2% by weight) in the liquid aprotic electrolyte effectively reduces the irreversible capacity loss associated with the bulk electrolyte reduction on graphite anodes. In general, SEI-forming additives are reduced at the negative electrode prior to the bulk electrolyte components due to their higher reductive potential [166]. The reduction process is accompanied by the formation of insoluble decomposition products that are immobilized at the anode/electrolyte interface in a film with thicknesses up to several tens of nanometers, thus shielding the bulk electrolyte from the charged electrode surface [166]. SEI-forming

Fig. 13 Different additive target functions in the LIB



additives not only reduce gas generation during the reduction process but also increase the stability of the SEI, e.g., at elevated temperatures [166].

The reaction mechanism of VC was elucidated by ab initio calculations to interpret and simulate XPS valence spectra to identify VC-derived decomposition products in the electrode/electrolyte interphases [167]. VC is radically polymerized on the anode surface, thus resulting in the formation of a thinner SEI when added to the conventional LiPF_6 /organic carbonate-based electrolyte (Fig. 14) [167]. However, theoretical modeling of the SEI, to obtain further insight into the interphasial structure, is rare [168–171].

Fluoroethylene carbonate (FEC) is the electrolyte additive most reported for SEI formation on silicon-based electrodes [172, 173]. The improvement mechanism of FEC is still under debate [127, 174, 175]. Recently, Tateyama et al. studied the decomposition of FEC by means of computational modelling and stressed the role of LiF in the SEI composition acting as a glue for the organic SEI components, especially on silicon-based electrodes [174]. However, the composition of the FEC-derived SEI, the chemical reactions involved, and the reaction intermediates remain to be elucidated [174]. Biphenyl (BP) is by far the most used shutdown additive to increase the intrinsic safety of the LIB. At the potential of 4.54 V vs. Li/Li^+ , BP is oxidized and forms a highly resistive cathode passivation film containing poly(p-phenylene) (Fig. 15) [176]. The co-generated protons diffuse to the anode side and are reduced to H_2 , leading to an increase in internal cell pressure [136]. At a defined pressure, the current interrupt device (CID) in the cell is activated and the current flow is interrupted [136]. Therefore, BP is used only in LIBs having a CID, e.g., in round cells.

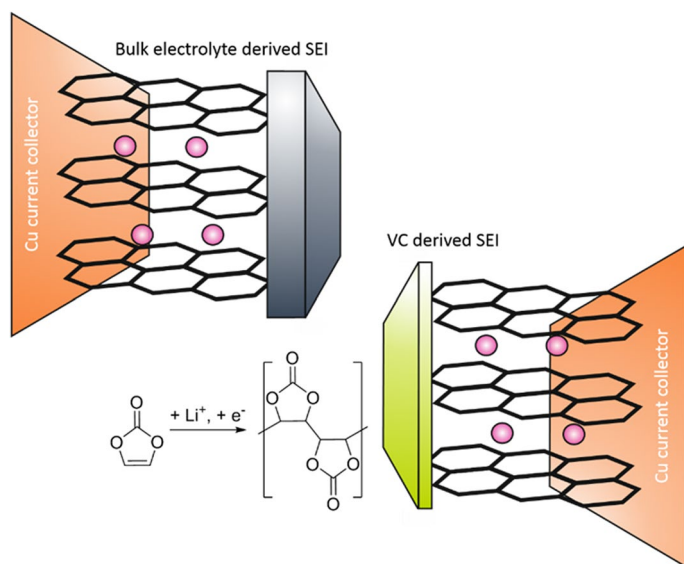


Fig. 14 Schematic illustration of vinylene carbonate (VC)-induced solid electrolyte interphase (SEI) formation

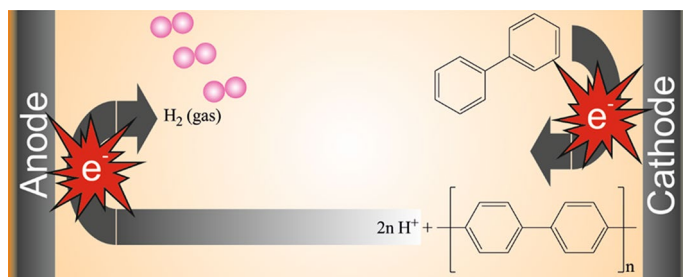


Fig. 15 Working principle of biphenyl (BP) as a shutdown additive

Due to the development of new cell chemistries, especially cathode materials with higher operation potentials, there is a need for the development of new shutdown additives with higher oxidation onset potential [177]. In this regard, quantum chemical calculations are useful screening tools with which to identify suitable candidates [176].

7 Conclusion

Regarding energy and power design, LIBs have a clear advantage compared to other secondary battery technologies. Yet, research into new electrode materials to further increase energy density, power density, cycle life and safety at affordable cost continues. The design and development of new electrode materials and electrolyte components based on understanding of operation and failure mechanisms of the battery, also at the electrolyte/electrode interfaces is important to further advance the limits of power, safety and cycle life in the LIB. Despite the fact that electrolyte belongs to the group of inactive materials in the LIB, the physicochemical properties and characteristics of the electrolyte/electrode interfaces formed significantly determine power and safety. Computational modeling of electrolytes provides significant insight into the electrochemical and transport properties of the bulk electrolyte and electrolyte decomposition reactions as well as the characteristics of the formed electrolyte/electrode interphases, which can effectively support research and development of new electrolyte components. Nevertheless, a link between predicted parameters and experimental values is always necessary to assess whether or not, and how accurately, any computational method and strategy can be used in a predictive manner.

References

1. Electrochemistry Dictionary and Encyclopedia (2014) The electrochemical society. <http://knowledge.electrochem.org/ed/dict.htm>
2. Zoski CG (2007) Handbook of electrochemistry. Elsevier, Amsterdam

3. Inzelt G, Lewenstam A, Scholz F (2013) Handbook of reference electrodes. Springer, Berlin
4. Scholz F (2009) Electroanalytical methods: guide to experiments and applications. Springer, Berlin
5. Srinivasan S (2006) Fuel cells: from fundamentals to applications. Springer, Berlin
6. Breitkopf C, Swider-Lyons K (2016) Springer handbook of electrochemical energy. Springer, Berlin
7. Brett CMA, Brett AMO (1993) Electrochemistry—principles, methods and applications. Oxford University Press, New York
8. Balzani V (2001) Electron transfer in chemistry: catalysis of electron transfer, heterogenous systems, gas-phase systems. Wiley, Amsterdam
9. Kuznetsov AM, Ulstrup J (1999) Electron transfer in chemistry and biology: an introduction to the theory. Wiley, Amsterdam
10. Taube H, Myers H, Rich RL (1953) *J Am Chem Soc* 75:4118. <https://doi.org/10.1021/ja01112a546>
11. Bard AJ, Faulkner LR (2000) Electrochemical methods: fundamentals and applications. Wiley, Amsterdam
12. Sharma P, Bhatti TS (2010) *Energy Convers Manag* 51:2901. <https://doi.org/10.1016/j.enconman.2010.06.031>
13. Simon P, Gogotsi Y (2008) *Nat Mater* 7:845
14. Wang G, Zhang L, Zhang J (2012) *Chem Soc Rev* 41:797
15. Frackowiak E, Béguin F (2001) *Carbon* 39:937. [https://doi.org/10.1016/S0008-6223\(00\)00183-4](https://doi.org/10.1016/S0008-6223(00)00183-4)
16. Zhang Y, Feng H, Wu X, Wang L, Zhang A, Xia T, Dong H, Li X, Zhang L (2009) *Int J Hydrogen Energy* 34:4889. <https://doi.org/10.1016/j.ijhydene.2009.04.005>
17. Zhong C, Deng Y, Hu W, Qiao J, Zhang L, Zhang J (2015) *Chem Soc Rev* 44:7484
18. Winter M, Besenhard JO (1999) *Chem Unserer Zeit* 33:252. <https://doi.org/10.1002/ciuz.19990330503>
19. Goodenough JB, Park K-S (2013) *J Am Chem Soc* 135:1167. <https://doi.org/10.1021/ja3091438>
20. Meister P, Jia H, Li J, Kloepsch R, Winter M, Placke T (2016) *Chem Mater* 28:7203. <https://doi.org/10.1021/acs.chemmater.6b02895>
21. Kasnatscheew J, Rodehorst U, Streipert B, Wiemers-Meyer S, Jakelski R, Wagner R, Laskovic IC, Winter M (2016) *J Electrochem Soc* 163:A2943. <https://doi.org/10.1149/2.0461614jes>
22. Goodenough JB, Kim Y (2009) *Chem Mater* 22:587. <https://doi.org/10.1021/cm901452z>
23. Kraysberg A, Ein-Eli Y (2012) *Adv Energy Mater* 2:922. <https://doi.org/10.1002/aenm.201200068>
24. Winter M, Brodd RJ (2004) *Chem Rev* 104:4245. <https://doi.org/10.1021/Cr020730k>
25. Reddy T (2010) Linden's handbook of batteries, 4th edn. McGraw-Hill, New York
26. Bieker P, Winter M (2016) *Chem Unserer Zeit* 50:26. <https://doi.org/10.1002/ciuz.201500713>
27. Winter M, Besenhard JO (1999) *Chem Unserer Zeit* 33:320. <https://doi.org/10.1002/ciuz.19990330603>
28. Palacin MR (2009) *Chem Soc Rev* 38:2565. <https://doi.org/10.1039/b820555h>
29. Bruce PG, Freunberger SA, Hardwick LJ, Tarascon J-M (2012) *Nat Mater* 11:19
30. Girishkumar G, McCloskey B, Luntz AC, Swanson S, Wilcke W (2010) *J Phys Chem Lett* 1:2193. <https://doi.org/10.1021/jz1005384>
31. Luntz AC, McCloskey BD (2014) *Chem Rev* 114:11721. <https://doi.org/10.1021/cr500054y>
32. Manthiram A, Fu Y, Su Y-S (2013) *Acc Chem Res* 46:1125. <https://doi.org/10.1021/ar300179v>
33. Manthiram A, Fu Y, Chung S-H, Zu C, Su Y-S (2014) *Chem Rev* 114:11751. <https://doi.org/10.1021/cr500062v>
34. Yabuuchi N, Kubota K, Dahbi M, Komaba S (2014) *Chem Rev* 114:11636. <https://doi.org/10.1021/cr500192f>
35. Saha P, Datta MK, Velikokhatnyi OI, Manivannan A, Alman D, Kumta PN (2014) *Prog Mater Sci* 66:1. <https://doi.org/10.1016/j.pmatsci.2014.04.001>
36. Muldoon J, Bucur CB, Gregory T (2014) *Chem Rev* 114:11683. <https://doi.org/10.1021/cr500049y>
37. Ponrouch A, Frontera C, Barde F, Palacin MR (2016) *Nat Mater* 15:169. <https://doi.org/10.1038/nmat4462>. <http://www.nature.com/nmat/journal/v15/n2/abs/nmat4462.html#supplementary-information>
38. Muldoon J, Bucur CB, Oliver AG, Sugimoto T, Matsui M, Kim HS, Allred GD, Zajicek J, Kotani Y (2012) *Energy Environ Sci* 5:5941. <https://doi.org/10.1039/c2ee03029b>
39. Jayaprakash N, Das SK, Archer LA (2011) *Chem Commun* 47:12610. <https://doi.org/10.1039/c1cc15779e>

40. Lin M-C, Gong M, Lu B, Wu Y, Wang D-Y, Guan M, Angell M, Chen C, Yang J, Hwang B-J, Dai H (2015) *Nature* 520:324. <https://doi.org/10.1038/nature14340>. <http://www.nature.com/nature/journal/v520/n7547/abs/nature14340.html#supplementary-information>
41. Rothermel S, Meister P, Schmuelling G, Fromm O, Meyer H-W, Nowak S, Winter M, Placke T (2014) *Energy Environ Sci* 7:3412. <https://doi.org/10.1039/c4ee01873g>
42. Placke T, Fromm O, Lux SF, Bieker P, Rothermel S, Meyer H-W, Passerini S, Winter M (2012) *J Electrochem Soc* 159:A1755. <https://doi.org/10.1149/2.011211jes>
43. Placke T, Bieker P, Lux SF, Fromm O, Meyer HW, Passerini S, Winter M (2012) *Zeitschrift für Physikalische Chemie. Int J Res Phys Chem Chem Phys* 226:391. <https://doi.org/10.1524/zpch.2012.0222>
44. Meister P, Fromm O, Rothermel S, Kasnatscheew J, Winter M, Placke T (2017) *Electrochim Acta* 228:18. <https://doi.org/10.1016/j.electacta.2017.01.034>
45. Liang Y, Tao Z, Chen J (2012) *Adv Energy Mater* 2:742. <https://doi.org/10.1002/aenm.201100795>
46. Speer ME, Kolek M, Jassoy JJ, Heine J, Winter M, Bieker PM, Esser B (2015) *Chem Commun* 51:15261. <https://doi.org/10.1039/c5cc04932f>
47. Bieker P, Winter M (2016) *Chem Unserer Zeit* 50:172. <https://doi.org/10.1002/ciuz.201600745>
48. Winter M, Placke T, Rothermel S, Meister P, Bar A, von Wedel W (2017) Elektromobilität—Was uns jetzt und künftig antreibt. BINE-Themeninfo I/2017. <https://www.bine.info/fileadmin/content/Publikationen/Themen-Infos/I2017/themen0117internetx.pdf>
49. Andre D, Kim S-J, Lamp P, Lux SF, Maglia F, Paschos O, Stiaszny B (2015) *J Mater Chem A* 3:6709. <https://doi.org/10.1039/c5ta00361j>
50. Besenhard JO, Winter M (1998) *Pure Appl Chem* 70:603
51. Winter M, Besenhard JO, Spahr ME, Novak P (1998) *Adv Mater* 10:725
52. Qi X, Blizanac B, DuPasquier A, Oljaca M, Li J, Winter M (2013) *Carbon* 64:334. <https://doi.org/10.1016/j.carbon.2013.07.083>
53. Qi X, Blizanac B, DuPasquier A, Meister P, Placke T, Oljaca M, Li J, Winter M (2014) *Phys Chem Chem Phys* 16:25306
54. Lux SF, Schappacher F, Balducci A, Passerini S, Winter M (2010) *J Electrochem Soc* 157:A320. <https://doi.org/10.1149/1.3291976>
55. Kasnatscheew J, Börner M, Streipert B, Meister P, Wagner R, Cekic Laskovic I, Winter M (2017) *J Power Sources* 362:278. <https://doi.org/10.1016/j.jpowsour.2017.07.044>
56. Krämer E, Schedlbauer T, Hoffmann B, Terborg L, Nowak S, Gores HJ, Passerini S, Winter M (2013) *J Electrochem Soc* 160:A356. <https://doi.org/10.1149/2.081302jes>
57. Wagner R, Preschitschek N, Passerini S, Leker J, Winter M (2013) *J Appl Electrochem* 43:481. <https://doi.org/10.1007/s10800-013-0533-6>
58. Meister P, Qi X, Kloepsch R, Krämer E, Streipert B, Winter M, Placke T (2017) *Chemoschem* 10:804. <https://doi.org/10.1002/cssc.201601636>
59. Streipert B, Roser S, Kasnatscheew J, Janssen P, Cao X, Wagner R, Cekic-Laskovic I, Winter M (2017) *J Electrochem Soc* 164:A1474. <https://doi.org/10.1149/2.0671707jes>
60. Bieker G, Winter M, Bieker P (2015) *Phys Chem Chem Phys* 17:8670. <https://doi.org/10.1039/c4cp05865h>
61. Ryou M-H, Lee YM, Lee Y, Winter M, Bieker P (2015) *Adv Funct Mater* 25:834. <https://doi.org/10.1002/adfm.201402953>
62. Heine J, Hilbig P, Qi X, Niehoff P, Winter M, Bieker P (2015) *J Electrochem Soc* 162:A1094. <https://doi.org/10.1149/2.0011507jes>
63. Winter M (2009) *Z Phys Chem* 223:1395. <https://doi.org/10.1524/zpch.2009.6086>
64. Rupp B, Schmuck M, Balducci A, Winter M, Kern W (2008) *Eur Polym J* 44:2986. <https://doi.org/10.1016/j.eurpolymj.2008.06.022>
65. Hovington P, Lagacé M, Guerfi A, Bouchard P, Mauger A, Julien CM, Armand M, Zaghib K (2015) *Nano Lett* 15:2671. <https://doi.org/10.1021/acs.nanolett.5b00326>
66. Kim T-H, Park J-S, Chang SK, Choi S, Ryu JH, Song H-K (2012) *Adv Energy Mater* 2:860. <https://doi.org/10.1002/aenm.201200028>
67. Kasavajjula U, Wang C, Appleby AJ (2007) *J Power Source* 163:1003. <https://doi.org/10.1016/j.jpowsour.2006.09.084>
68. Winter M, Besenhard JO (1999) *Electrochim Acta* 45:31. [https://doi.org/10.1016/s0013-4686\(99\)00191-7](https://doi.org/10.1016/s0013-4686(99)00191-7)
69. Zhang W-J (2011) *J Power Source* 196:13. <https://doi.org/10.1016/j.jpowsour.2010.07.020>

70. Park C-M, Kim J-H, Kim H, Sohn H-J (2010) *Chem Soc Rev* 39:3115. <https://doi.org/10.1039/b919877f>
71. Obrovac MN, Chevrier VL (2014) *Chem Rev* 114:11444. <https://doi.org/10.1021/cr500207g>
72. Winter M, Besenhard J, Albering J, Yang J, Wachtler M (1998) *Progress Battery Battery Mater* 17:208
73. Cabana J, Monconduit L, Larcher D, Palacin MR (2010) *Adv Mater* 22:E170
74. Reddy MV, Subba Rao GV, Chowdari BVR (2013) *Chem Rev* 113:5364. <https://doi.org/10.1021/cr3001884>
75. Jia H, Kloepsch R, He X, Evertz M, Nowak S, Li J, Winter M, Placke T (2016) *Acta Chim Slov* 63:470
76. Flandrois S, Simon B (1999) *Carbon* 37:165. [https://doi.org/10.1016/S0008-6223\(98\)00290-5](https://doi.org/10.1016/S0008-6223(98)00290-5)
77. Kohs W, Santner HJ, Hofer F, Schrottner H, Doninger J, Barsukov I, Buqa H, Albering JH, Moller KC, Besenhard JO, Winter M (2003) *J Power Source* 119:528. [https://doi.org/10.1016/s0378-7753\(03\)00278-7](https://doi.org/10.1016/s0378-7753(03)00278-7)
78. Huggins R (2008) *Advanced batteries: materials science aspects*. Springer, New York
79. Winter M, Besenhard JO (2011) *Handbook of battery materials*. Wiley, Amsterdam, p 433
80. Wang Y, Nakamura S, Ue M, Balbuena PB (2001) *J Am Chem Soc* 123:11708. <https://doi.org/10.1021/ja0164529>
81. Wang YX, Nakamura S, Tasaki K, Balbuena PB (2002) *J Am Chem Soc* 124:4408. <https://doi.org/10.1021/ja017073i>
82. Placke T, Siozios V, Rothermel S, Meister P, Colle C, Winter M (2015) *Z Phys Chem* 229:1451
83. Placke T, Siozios V, Schmitz R, Lux SF, Bieker P, Colle C, Meyer HW, Passerini S, Winter M (2012) *J Power Source* 200:83. <https://doi.org/10.1016/j.jpowsour.2011.10.085>
84. Schmitz RW, Murmann P, Schmitz R, Müller R, Krämer L, Kasnatscheew J, Isken P, Niehoff P, Nowak S, Röschenhaler G-V, Ignatiev N, Sartori P, Passerini S, Kunze M, Lex-Balducci A, Schreiner C, Cekic-Laskovic I, Winter M (2014) *Prog Solid State Chem* 42:65. <https://doi.org/10.1016/j.progsolidstchem.2014.04.003>
85. Wagner R, Brox S, Kasnatscheew J, Gallus DR, Amereller M, Cekic-Laskovic I, Winter M (2014) *Electrochem Commun* 40:80. <https://doi.org/10.1016/j.elecom.2014.01.004>
86. Kasnatscheew J, Schmitz RW, Wagner R, Winter M, Schmitz R (2013) *J Electrochem Soc* 160:A1369. <https://doi.org/10.1149/2.009309jes>
87. Winter M, Moeller K-C, Besenhard JO (2003) Carbonaceous and graphitic anodes. In: Nazri G-A, Pistoia G (eds) *Lithium batteries: science and technology*. Springer, Boston, p 145
88. Börner M, Klamor S, Hoffmann B, Schroeder M, Nowak S, Würsig A, Winter M, Schappacher FM (2016) *J Electrochem Soc* 163:A831. <https://doi.org/10.1149/2.0191606jes>
89. Cao X, He X, Wang J, Liu H, Röser S, Rad BR, Evertz M, Streipert B, Li J, Wagner R, Winter M, Cekic-Laskovic I (2016) *ACS Appl Mater Interface* 8:25971. <https://doi.org/10.1021/acsami.6b07687>
90. Yi T-F, Jiang L-J, Shu J, Yue C-B, Zhu R-S, Qiao H-B (2010) *J Phys Chem Solids* 71:1236. <https://doi.org/10.1016/j.jpcc.2010.05.001>
91. Sun X, Radovanovic PV, Cui B (2015) *New J Chem* 39:38. <https://doi.org/10.1039/c4nj01390e>
92. Nitta N, Wu F, Lee JT, Yushin G (2015) *Mater Today* 18:252. <https://doi.org/10.1016/j.mattod.2014.10.040>
93. Xu B, Qian D, Wang Z, Meng YS (2012) *Mater Sci Eng R Rep* 73:51
94. Masquelier C, Croguennec L (2013) *Chem Rev* 113:6552. <https://doi.org/10.1021/cr3001862>
95. Ellis BL, Lee KT, Nazar LF (2010) *Chem Mater* 22:691. <https://doi.org/10.1021/cm902696j>
96. Kasnatscheew J, Evertz M, Streipert B, Wagner R, Klöpsch R, Vortmann B, Hahn H, Nowak S, Amereller M, Gentschev AC, Lamp P, Winter M (2016) *Phys Chem Chem Phys* 18:3956. <https://doi.org/10.1039/c5cp07718d>
97. Ohzuku T, Brodd RJ (2007) *J Power Source* 174:449. <https://doi.org/10.1016/j.jpowsour.2007.06.154>
98. Wagner R, Streipert B, Kraft V, Reyes Jiménez A, Röser S, Kasnatscheew J, Gallus DR, Börner M, Mayer C, Arlinghaus HF, Korth M, Amereller M, Cekic-Laskovic I, Winter M (2016) *Adv Mater Interface* 3:1600096. <https://doi.org/10.1002/admi.201600096>
99. Gallus DR, Wagner R, Wiemers-Meyer S, Winter M, Cekic-Laskovic I (2015) *Electrochim Acta* 184:410. <https://doi.org/10.1016/j.electacta.2015.10.002>
100. Buchberger I, Seidlmayer S, Pokharel A, Piana M, Hattendorff J, Kudejova P, Gilles R, Gasteiger HA (2015) *J Electrochem Soc* 162:A2737. <https://doi.org/10.1149/2.0721514jes>

101. Kasnatscheew J, Evertz M, Kloepsch R, Streipert B, Wagner R, Cekic Laskovic I, Winter M (2017) *Energy Technol* 5:1670. <https://doi.org/10.1002/ente.201700068>
102. Kasnatscheew J, Evertz M, Streipert B, Wagner R, Nowak S, Cekic Laskovic I, Winter M (2017) *J Phys Chem C* 121:1521. <https://doi.org/10.1021/acs.jpcc.6b11746>
103. Wagner R, Kraft V, Streipert B, Kasnatscheew J, Gallus DR, Amereller M, Korth M, Cekic-Laskovic I, Winter M (2017) *Electrochim Acta* 228:9. <https://doi.org/10.1016/j.electacta.2017.01.029>
104. Chen Z, Qin Y, Amine K, Sun YK (2010) *J Mater Chem* 20:7606. <https://doi.org/10.1039/c0jm00154f>
105. Fu LJ, Liu H, Li C, Wu YP, Rahm E, Holze R, Wu HQ (2006) *Solid State Sci* 8:113. <https://doi.org/10.1016/j.solidstatesciences.2005.10.019>
106. Krueger S, Kloepsch R, Li J, Nowak S, Passerini S, Winter M (2013) *J Electrochem Soc* 160:A542. <https://doi.org/10.1149/2.022304jes>
107. Kasnatscheew J, Evertz M, Streipert B, Wagner R, Nowak S, Cekic Laskovic I, Winter M (2017) *J Power Source* 359:458. <https://doi.org/10.1016/j.jpowsour.2017.05.092>
108. He P, Yu HJ, Li D, Zhou HS (2012) *J Mater Chem* 22:3680. <https://doi.org/10.1039/C2jm14305d>
109. Manthiram A, Choi J, Choi W (2006) *Solid State Ion* 177:2629. <https://doi.org/10.1016/j.ssi.2006.02.041>
110. Reed J, Ceder G, Van der Ven A (2001) *Electrochem Solid State Lett* 4:A78. <https://doi.org/10.1149/1.1368896>
111. Chebiam RV, Kannan AM, Prado F, Manthiram A (2001) *Electrochem Commun* 3:624. [https://doi.org/10.1016/s1388-2481\(01\)00232-6](https://doi.org/10.1016/s1388-2481(01)00232-6)
112. Liu W, Oh P, Liu X, Lee MJ, Cho W, Chae S, Kim Y, Cho J (2015) *Angew Chem Int Ed* 54:4440. <https://doi.org/10.1002/anie.201409262>
113. Ohzuku T, Makimura Y (2001) Layered lithium insertion material of LiNi 1/2Mn 1/2O2: A possible alternative to LiCoO2 for advanced lithium-ion batteries. *Chem Lett* 30:744–745
114. Zhecheva E, Stoyanova R (1993) *Solid State Ion* 66:143. [https://doi.org/10.1016/0167-2738\(93\)90037-4](https://doi.org/10.1016/0167-2738(93)90037-4)
115. Whittingham MS (2004) *Chem Rev* 104:4271. <https://doi.org/10.1021/Cr020731c>
116. Rozier P, Tarascon JM (2015) *J Electrochem Soc* 162:A2490. <https://doi.org/10.1149/2.0111514jes>
117. Li J, Kloepsch R, Stan MC, Nowak S, Kunze M, Winter M, Passerini S (2011) *J Power Source* 196:4821. <https://doi.org/10.1016/j.jpowsour.2011.01.006>
118. Kasnatscheew J, Placke T, Streipert B, Rothermel S, Wagner R, Meister P, Laskovic IC, Winter M (2017) *J Electrochem Soc* 164:A2479. <https://doi.org/10.1149/2.0961712jes>
119. Kang K, Meng YS, Bréger J, Grey CP, Ceder G (2006) *Science* 311:977
120. Fergus JW (2010) *J Power Source* 195:4554. <https://doi.org/10.1016/j.jpowsour.2010.01.076>
121. Long L, Wang S, Xiao M, Meng Y (2016) *J Mater Chem A* 4:10038. <https://doi.org/10.1039/c6ta02621d>
122. Quartarone E, Mustarelli P (2011) *Chem Soc Rev* 40:2525
123. Armand M, Endres F, MacFarlane DR, Ohno H, Scrosati B (2009) *Nat Mater* 8:621
124. Lewandowski A, Świdarska-Mocek A (2009) *J Power Source* 194:601. <https://doi.org/10.1016/j.jpowsour.2009.06.089>
125. Xu K (2004) *Chem Rev* 104:4303. <https://doi.org/10.1021/Cr030203g>
126. Jow TR, Xu K, Borodin O, Makoto U (2014) *Electrolytes for lithium and lithium-ion batteries*. Springer, New York
127. Xu K (2014) *Chem Rev* 114:11503. <https://doi.org/10.1021/cr500003w>
128. Amereller M, Schedlbauer T, Moosbauer D, Schreiner C, Stock C, Wudy F, Zugmann S, Hammer H, Maurer A, Gschwind RM, Wiemhofer HD, Winter M, Gores HJ (2014) *Prog Solid State Chem* 42:39. <https://doi.org/10.1016/j.progsolidstchem.2014.04.001>
129. Wang Y, Yi J, Xia Y (2012) *Adv Energy Mater* 2:830. <https://doi.org/10.1002/aenm.201200065>
130. Li Q, Chen J, Fan L, Kong X, Lu Y (2016) *Green Energy Environ* 1:18. <https://doi.org/10.1016/j.gee.2016.04.006>
131. Ozawa K (1994) *Solid State Ionics* 69:212. [https://doi.org/10.1016/0167-2738\(94\)90411-1](https://doi.org/10.1016/0167-2738(94)90411-1)
132. Izutsu K (2009) *Electrochemistry in nonaqueous solutions*. Wiley, Amsterdam
133. Borodin O, Smith GD (2009) *J Phys Chem B* 113:1763. <https://doi.org/10.1021/jp809614h>
134. von Wald Cresce A, Borodin O, Xu K (2012) *J Phys Chem C* 116:26111. <https://doi.org/10.1021/jp303610t>
135. Borodin O (2014) Molecular modeling of electrolytes. In: Jow TR, Xu K, Borodin O, Ue M (eds) *Electrolytes for lithium and lithium-ion batteries*. Springer, New York, pp 371–402

136. Cekic-Laskovic I, von Aspern N, Imholt L, Kaymaksiz S, Oldiges K, Rad BR, Winter M (2017) *Top Curr Chem* 375:37
137. Brox S, Röser S, Husch T, Hildebrand S, Fromm O, Korth M, Winter M, Cekic-Laskovic I (2016) *Chemosuschem* 9:1704. <https://doi.org/10.1002/cssc.201600369>
138. Husch T, Yilmazer ND, Balducci A, Korth M (2015) *Phys Chem Chem Phys* 17:3394. <https://doi.org/10.1039/c4cp04338c>
139. Wagner R, Korth M, Streipert B, Kasnatscheew J, Gallus DR, Brox S, Amereller M, Cekic-Laskovic I, Winter M (2016) *ACS Appl Mater Interface* 8:30871. <https://doi.org/10.1021/acsami.6b09164>
140. Nowak S, Winter M (2015) *J Electrochem Soc* 162:A2500. <https://doi.org/10.1149/2.0121514jes>
141. Kraft V, Weber W, Streipert B, Wagner R, Schultz C, Winter M, Nowak S (2016) *RSC Adv* 6:8. <https://doi.org/10.1039/c5ra23624j>
142. Weber W, Wagner R, Streipert B, Kraft V, Winter M, Nowak S (2016) *J Power Source* 306:193. <https://doi.org/10.1016/j.jpowsour.2015.12.025>
143. Weber W, Kraft V, Grützke M, Wagner R, Winter M, Nowak S (2015) *J Chromatogr A* 1394:128. <https://doi.org/10.1016/j.chroma.2015.03.048>
144. Kraft V, Grützke M, Weber W, Menzel J, Wiemers-Meyer S, Winter M, Nowak S (2015) *J Chromatogr A* 1409:201. <https://doi.org/10.1016/j.chroma.2015.07.054>
145. Verma P, Maire P, Novák P (2010) *Electrochim Acta* 55:6332. <https://doi.org/10.1016/j.electacta.2010.05.072>
146. Gauthier M, Carney TJ, Grimaud A, Giordano L, Pour N, Chang H-H, Fenning DP, Lux SF, Paschos O, Bauer C, Maglia F, Lupart S, Lamp P, Shao-Horn Y (2015) *J Phys Chem Lett* 6:4653. <https://doi.org/10.1021/acs.jpcclett.5b01727>
147. Ue M, Murakami A, Nakamura S (2002) *J Electrochem Soc* 149:A1572. <https://doi.org/10.1149/1.1517579>
148. Johansson P (2006) *J Phys Chem A* 110:12077. <https://doi.org/10.1021/jp0653297>
149. Shao N, Sun X-G, Dai S, Jiang D-E (2011) *J Phys Chem B* 115:12120. <https://doi.org/10.1021/jp204401t>
150. Zhang X, Pugh JK, Ross PN (2001) *J Electrochem Soc* 148:E183. <https://doi.org/10.1149/1.1362546>
151. Assary RS, Curtiss LA, Redfern PC, Zhang Z, Amine K (2011) *J Phys Chem C* 115:12216. <https://doi.org/10.1021/jp2019796>
152. Borodin O, Behl W, Jow TR (2013) *J Phys Chem C* 117:8661. <https://doi.org/10.1021/jp400527c>
153. Kasnatscheew J, Streipert B, Röser S, Wagner R, Cekic Laskovic I, Winter M (2017) *Phys Chem Chem Phys* 19:16078. <https://doi.org/10.1039/C7CP03072J>
154. Xing L, Borodin O, Smith GD, Li W (2011) *J Phys Chem A* 115:13896. <https://doi.org/10.1021/jp206153n>
155. Yoshitake H, Abe K, Kitakura T, Gong JB, Lee YS, Nakamura H, Yoshio M (2003) *Chem Lett* 32:134
156. Xing L, Li W, Wang C, Gu F, Xu M, Tan C, Yi J (2009) *J Phys Chem B* 113:16596. <https://doi.org/10.1021/jp9074064>
157. Xing L, Wang C, Li W, Xu M, Meng X, Zhao S (2009) *J Phys Chem B* 113:5181. <https://doi.org/10.1021/jp810279h>
158. Scheers J, Johansson P (2014) Prediction of electrolyte and additive electrochemical stabilities. In: Jow TR, Xu K, Borodin O, Ue M (eds) *Electrolytes for lithium and lithium-ion batteries*. Springer, New York, p 403
159. Tan S, Ji YJ, Zhang ZR, Yang Y (2014) *ChemPhysChem* 15:1956. <https://doi.org/10.1002/cphc.201402175>
160. Zhang Z, Hu L, Wu H, Weng W, Koh M, Redfern PC, Curtiss LA, Amine K (2013) *Energy Environ Sci* 6:1806. <https://doi.org/10.1039/c3ee24414h>
161. Böttcher T, Duda B, Kalinovich N, Kazakova O, Ponomarenko M, Vlasov K, Winter M, Röschenhaler GV (2014) *Prog Solid State Chem* 42:202. <https://doi.org/10.1016/j.progsolidschem.2014.04.013>
162. Böttcher T, Kalinovich N, Kazakova O, Ponomarenko M, Vlasov K, Winter M, Röschenhaler GV (2015) Chapter 6—Novel fluorinated solvents and additives for lithium-ion batteries. In: Groult H (ed) *Advanced fluoride-based materials for energy conversion*. Elsevier, New York, pp 125–145
163. Abouimrane A, Belharouak I, Amine K (2009) *Electrochem Commun* 11:1073. <https://doi.org/10.1016/j.elecom.2009.03.020>

164. Duncan H, Salem N, Abu-Lebdeh Y (2013) *J Electrochem Soc* 160:A838. <https://doi.org/10.1149/2.088306jes>
165. Isken P, Dippel C, Schmitz R, Schmitz RW, Kunze M, Passerini S, Winter M, Lex-Balducci A (2011) *Electrochim Acta* 56:7530. <https://doi.org/10.1016/j.electacta.2011.06.095>
166. Zhang SS (2006) *J Power Source* 162:1379. <https://doi.org/10.1016/j.jpowsour.2006.07.074>
167. El Ouatani L, Dedryvere R, Siret C, Biensan P, Reynaud S, Iratcabal P, Gonbeau D (2009) *J Electrochem Soc* 156:A103. <https://doi.org/10.1149/1.3029674>
168. Jorn R, Kumar R, Abraham DP, Voth GA (2013) *J Phys Chem C* 117:3747. <https://doi.org/10.1021/jp3102282>
169. Leung K (2013) *J Phys Chem C* 117:1539. <https://doi.org/10.1021/jp308929a>
170. Single F, Horstmann B, Latz A (2017) *J Electrochem Soc* 164:E3132. <https://doi.org/10.1149/2.0121711jes>
171. Single F, Horstmann B, Latz A (2016) *Phys Chem Chem Phys* 18:17810. <https://doi.org/10.1039/c6cp02816k>
172. Zhang S, He M, Su C-C, Zhang Z (2016) *Curr Opin Chem Eng* 13:24. <https://doi.org/10.1016/j.coche.2016.08.003>
173. Reyes Jiménez A, Klöpsch R, Wagner R, Rodehorst UC, Kolek M, Nölle R, Winter M, Placke T (2017) *ACS Nano*. <https://doi.org/10.1021/acsnano.7b00922>
174. Okuno Y, Ushirogata K, Sodeyama K, Tateyama Y (2016) *Phys Chem Chem Phys* 18:8643. <https://doi.org/10.1039/c5cp07583a>
175. Profatlova IA, Stock C, Schmitz A, Passerini S, Winter M (2013) *J Power Source* 222:140. <https://doi.org/10.1016/j.jpowsour.2012.08.066>
176. Wilken S, Johansson P, Jacobsson P (2013) *Lithium batteries*. Wiley, Amsterdam, p 39
177. Streipert B, Janßen P, Cao X, Kasnatscheew J, Wagner R, Cekic-Laskovic I, Winter M, Placke T (2017) *J Electrochem Soc* 164:A168. <https://doi.org/10.1149/2.0711702jes>